Biomedical Optics EXPRESS

Effect of number density on optimal design of gold nanoshells for plasmonic photothermal therapy

Debabrata Sikdar,[1] Ivan D. Rukhlenko,[1,*] Wenlong Cheng,[2,3] and Malin Premaratne[1]

[1]*Advanced Computing and Simulation Laboratory (AχL), Department of Electrical and Computer Systems Engineering, Monash University, Clayton 3800, Victoria, Australia*
[2]*Department of Chemical Engineering, Faculty of Engineering, Monash University, Clayton 3800, Victoria, Australia*
[3]*The Melbourne Centre for Nanofabrication, 151 Wellington Road, Clayton 3168, Victoria, Australia*
**ivan.rukhlenko @monash.edu*

Abstract: Despite much research efforts being devoted to the design optimization of metallic nanoshells, no account is taken of the fact that the number of the nanoshells that can be delivered to a given cancerous site vary with their size. In this paper, we study the effect of the nanoshell number density on the absorption and scattering properties of a gold-nanoshell ensemble exposed to a broadband near-infrared radiation, and optimize the nanoshells' dimensions for efficient cancer treatment by analyzing a wide range of human tissues. We first consider the general situation in which the number of the delivered nanoshells decreases with their mean radius R as $\propto R^{-\beta}$, and demonstrate that the optimal design of nanoshells required to treat cancer most efficiently depends critically on β. In the case of $\beta = 2$, the maximal energy absorbed (scattered) by the ensemble is achieved for the same dimensions that maximize the absorption (scattering) efficiency of a single nanoshell. We thoroughly study this special case by the example of gold nanoshells with silica core. To ensure that minimal thermal injury is caused to the healthy tissue surrounding a cancerous site, we estimate the optimal dimensions that minimize scattering by the nanoshells for a desired value of the absorption efficiency. The comparison of gold nanoshells with different cores shows that hollow nanoshells exhibiting relatively low absorption efficiency are less harmful to the healthy tissue and, hence, are preferred over the strongly absorbing nanoshells. For each of the cases analyzed, we provide approximate analytical expressions for the optimal nanoshell dimensions, which may be used as design guidelines by experimentalists, in order to optimize the synthesis of gold nanoshells for treating different types of human cancer at their various growth stages.

OCIS codes: (170.0170) Medical optics and biotechnology; (160.4236) Nanomaterials; (250.5403) Plasmonics; (350.5340) Photothermal effects.

References and links

1. S. J. Tan, M. J. Campolongo, D. Luo, and W. Cheng, "Building plasmonic nanostructures with DNA," Nat. Nanotechnol. **6**, 268–276 (2011).

#178972 - $15.00 USD Received 31 Oct 2012; revised 29 Nov 2012; accepted 29 Nov 2012; published 5 Dec 2012

2. V. P. Pattani and J. W. Tunnell, "Nanoparticle-mediated photothermal therapy: A comparative study of heating for different particle types," Lasers Surg. Med. **44**, 675–684 (2012).
3. L. C. Kennedy, L. R. Bickford, N. A. Lewinski, A. J. Coughlin, Y. Hu, E. S. Day, J. L. West, and R. A. Drezek, "A new era for cancer treatment: Gold-nanoparticle-mediated thermal therapies," Small **7**, 169–183 (2011).
4. J. Chen, C. Glaus, R. Laforest, Q. Zhang, M. Yang, M. Gidding, M. J. Welch, and Y. Xia, "Gold nanocages as photothermal transducers for cancer treatment," Small **6**, 811–817 (2010).
5. S. Lal, S. E. Clare, and N. J. Halas, "Nanoshell-enabled photothermal cancer therapy: Impending clinical impact," Acc. Chem. Res. **41**, 1842–1851 (2008).
6. M. P. Melancon, W. Lu, Z. Yang, R. Zhang, Z. Cheng, A. M. Elliot, J. Stafford, T. Olson, J. Z. Zhang, and C. Li, "In vitro and in vivo targeting of hollow gold nanoshells directed at epidermal growth factor receptor for photothermal ablation therapy," Mol. Cancer Ther. **7**, 1730–1739 (2008).
7. X. Huang, P. K. Jain, I. H. El-Sayed, and M. A. El-Sayed, "Plasmonic photothermal therapy (PPTT) using gold nanoparticles," Lasers Med. Sci. **23**, 217–228 (2008).
8. C. Loo, A. Lin, L. Hirsch, M. H. Lee, J. Barton, N. Halas, J. West, and R. Drezek, "Nanoshell-enabled photonics-based imaging and therapy of cancer," Technol. Cancer Res. Treat. **3**, 33–40 (2004).
9. V. U. Fiedler, H. J. Schwarzmaier, F. Eickmeyer, F. P. Muller, C. Schoepp, and P. R. Verreet, "Laser-induced interstitial thermotherapy of liver metastases in an interventional 0.5 Tesla MRI system: Technique and first clinical experiences," J. Magn. Reson. Imaging **13**, 729–737 (2001).
10. F. Y. Cheng, C. T. Chen, and C. S. Yeh, "Comparative efficiencies of photothermal destruction of malignant cells using antibody-coated silica@Au nanoshells, hollow Au/Ag nanospheres and Au nanorods," Nanotechnol. **20**, 425104 (2009).
11. T. A. Erickson and J. W. Tunnell, "Gold nanoshells in biomedical applications," in *Mixed Metal Nanomaterials*, C. S. S. R. Kumar, ed., Vol. 3 of Nanomaterials for the Life Sciences (Wiley-VCH, Weinheim, 2009), pp. 1–44.
12. P. Puvanakrishnan, J. Park, D. Chatterjee, S. Krishnan, and J. W. Tunnell, "In vivo tumor targeting of gold nanoparticles: Effect of particle type and dosing strategy," Int. J. Nanomed. **7**, 1251–1258 (2012).
13. S. Y. Liu, Z. S. Liang, F. Gao, S. F. Luo, and G. Q. Lu, "In vitro photothermal study of gold nanoshells functionalized with small targeting peptides to liver cancer cells," J. Mater. Sci. Mater. Med. **21**, 665–674 (2010).
14. R. J. Bernardi, A. R. Lowery, P. A. Thompson, S. M. Blaney, and J. L. West, "Immunonanoshells for targeted photothermal ablation in medulloblastoma and glioma: an in vitro evaluation using human cell lines," J. Neurooncol. **86**, 165–172 (2008).
15. A. M. Gobin, J. J. Moon, and J. L. West, "EphrinAl-targeted nanoshells for photothermal ablation of prostate cancer cells," Int. J. Nanomed. **3**, 351–358 (2008).
16. J. M. Stern, J. Stanfield, Y. Lotan, S. Park, J. T. Hsieh, and J. A. Cadeddu, "Efficacy of laser-activated gold nanoshells in ablating prostate cancer cells in vitro," J. Endourol. **21**, 939–943 (2007).
17. A. R. Lowery, A. M. Gobin, E. S. Day, N. J. Halas, and J. L. West, "Immunonanoshells for targeted photothermal ablation of tumor cells," Int. J. Nanomed. **1**, 149–154 (2006).
18. L. R. Hirsch, R. J. Stafford, J. A. Bankson, S. R. Sershen, B. Rivera, R. E. Price, J. D. Hazle, N. J. Halas, and J. L. West, "Nanoshell-mediated near-infrared thermal therapy of tumors under magnetic resonance guidance," Proc. Natl. Acad. Sci. U.S.A. **100**, 13549–13554 (2003).
19. J. Z. Zhang, "Biomedical applications of shape-controlled plasmonic nanostructures: A case study of hollow gold nanospheres for photothermal ablation therapy of cancer," J. Phys. Chem. Lett. **1**, 686–695 (2010).
20. X. Huang and M. A. El-Sayed, "Gold nanoparticles: Optical properties and implementations in cancer diagnosis and photothermal therapy," J. Adv. Res. **1**, 13–28 (2010).
21. O. Pena, U. Pal, L. Rodriguez-Fernandez, and A. Crespo-Sosa, "Linear optical response of metallic nanoshells in different dielectric media," J. Opt. Soc. Am. B **25**, 1371–1379 (2008).
22. P. K. Jain, K. S. Lee, I. H. El-Sayed, and M. A. El-Sayed, "Calculated absorption and scattering properties of gold nanoparticles of different size, shape, and composition: Applications in biological imaging and biomedicine," J. Phys. Chem. B **110**, 7238–7248 (2006).
23. R. D. Averitt, S. L. Westcott, and N. J. Halas, "Linear optical properties of gold nanoshells," J. Opt. Soc. Am. B **16**, 1824–1832 (1999).
24. A. E. Neeves and M. H. Birnboim, "Composite structures for the enhancement of nonlinear-optical susceptibility," J. Opt. Soc. Am. B **6**, 787–796 (1989).
25. S. Kessentini and D. Barchiesi, "Quantitative comparison of optimized nanorods, nanoshells and hollow nanospheres for photothermal therapy," Biomed. Opt. Express **3**, 590–604 (2012).
26. T. Grosges, D. Barchiesi, S. Kessentini, G. Grehan, and M. L. de la Chapelle, "Nanoshells for photothermal therapy: A Monte-Carlo based numerical study of their design tolerance," Biomed. Opt. Express **2**, 1584–1596 (2011).
27. J. F. Lovell, C. S. Jin, E. Huynh, H. Jin, C. Kim, J. L. Rubinstein, W. C. W. Chan, W. Cao, L. V. Wang, and G. Zheng, "Porphysome nanovesicles generated by porphyrin bilayers for use as multimodal biophotonic contrast agents," Nat. Mater. **10**, 324–332 (2011).
28. J. Park, A. Estrada, J. A. Schwartz, P. Diagaradjane, S. Krishnan, C. Coleman, J. D. Payne, A. K. Dunn, and J. W. Tunnell, "Two-photon-induced photoluminescence imaging of gold nanoshell's tumor biodistribution,"

#178972 - $15.00 USD Received 31 Oct 2012; revised 29 Nov 2012; accepted 29 Nov 2012; published 5 Dec 2012

Proc. SPIE **7192**, 71920T (2009).
29. B. Choi and A. J. Welch, "Analysis of thermal relaxation during laser irradiation of tissue," Lasers Surg. Med. **29**, 351–359 (2001).
30. X. Zheng and F. Zhou, "Noncovalent functionalization of single-walled carbon nanotubes by indocyanine green: Potential nanocomplexes for photothermal therapy," J. X-Ray Sci. Tech. **19**, 275–284 (2011).
31. V. V. Tuchin, *Tissue Optics: Light Scattering Methods and Instruments for Medical Diagnosis*, 2nd ed. (SPIE Publications, Bellingham, Washington, 2007).
32. C. C. Handapangoda, M. Premaratne, D. M. Paganin, and P. R. D. S. Hendahewa, "Technique for handling wave propagation specific effects in biological tissue: mapping of the photon transport equation to Maxwell's equations," Opt. Express **16**, 17792–17807 (2008).
33. M. Premaratne, E. Premaratne, and A. Lowery, "The photon transport equation for turbid biological media with spatially varying isotropic refractive index," Opt. Express **13**, 389–399 (2005).
34. C. F. Bohren and D. R. Huffman, *Absorption and Scattering of Light by Small Particles* (Wiley, New York, 1998).
35. C. Liu, C. C. Mi, and B. Q. Li, "Energy absorption of gold nanoshells in hyperthermia therapy," IEEE Trans. Nanobiosci. **7**, 206–214 (2008).
36. M. L. Marasinghe, M. Premaratne, D. M. Paganin, and M. A. Alonso, "Coherence vortices in Mie scattered nonparaxial partially coherent beams," Opt. Express **20**, 2858–2875 (2012).
37. M. L. Marasinghe, M. Premaratne, and D. M. Paganin, "Coherence vortices in Mie scattering of statistically stationary partially coherent fields," Opt. Express **18**, 6628–6641 (2010).
38. A. N. Rubinov and A. A. Afanas'ev, "Nonresonance mechanisms of biological effects of coherent and incoherent light," Opt. Spectrosc. **98**, 943–948 (2005).
39. R. Fiolka, K. Si, and M. Cui, "Complex wavefront corrections for deep tissue focusing using low coherence backscattered light," Opt. Express **20**, 16532–16543 (2012).
40. N. W. Ashcroft and N. D. Mermin, *Solid State Physics* (Holt-Saunders, Philadelphia, 1976).
41. U. Kreibig and L. Genzel, "Optical absorption of small metallic particles," Surf. Sci. **156**, 678–700 (1985).
42. P. B. Johnson and R. W. Christy, "Optical constants of the noble metals," Phys. Rev. B **6**, 4370–4379 (1972).
43. S. N. Il'chenko, Y. O. Kostin, I. A. Kukushkin, M. A. Ladugin, P. I. Lapin, A. A. Lobintsov, A. A. Marmalyuk, and S. D. Yakubovich, "Broadband superluminescent diodes and semiconductor optical amplifiers for the spectral range 750–800 nm," Quantum Electron. **41**, 677–680 (2011).
44. C. E. Dimas, C. L. Tan, H. S. Djie, and B. S. Ooi, "Coherence length characteristics from broadband semiconductor emitters: superluminescent diodes versus broadband laser diodes," Proc. SPIE 7230, 72300B (2009).
45. J. M. Schmitt, "Optical coherence tomography (OCT): A review," IEEE J. Sel. Top. Quantum Electron. **5**, 1205–1215 (1999).
46. G. A. Alphonse, D. B. Gilbert, M. G. Harvey, and M. Ettenberg, "High-power superluminescent diodes," IEEE J. Quantum Electron. **24**, 2454–2457 (1988).
47. P. Cimalla, J. Walther, M. Mehner, M. Cuevas, and E. Koch, "Simultaneous dual-band optical coherence tomography in the spectral domain for high resolution in vivo imaging," Opt. Express **17**, 19486–19500 (2009).
48. X. Huang, I. H. El-Sayed, and M. A. El-Sayed, "Gold nanoparticles for plasmonic photothermal cancer therapy," in "Handbook of Nanophysics," K. D. Sattler, ed. (CRC Press, 2010), pp. 1–15.
49. I. H. Malitson, "Interspecimen comparison of the refractive index of fused silica," J. Opt. Soc. Am. **55**, 1205–1208 (1965).
50. G. Wu, A. Mikhailovsky, H. A. Khant, and J. A. Zasadzinski, "Synthesis, characterization, and optical response of gold nanoshells used to trigger release from liposomes," Methods Enzymol. **464**, 279–307 (2009).
51. V. V. Tuchin, "Optical clearing of tissues and blood using the immersion method," J. Phys. D: Appl. Phys. **38**, 2497–2518 (2005).
52. F. A. Duck, *Physical Properties of Tissue: a Comprehensive Reference Book* (Academic, London, 1990).
53. E. Prodan, C. Radloff, N. J. Halas, and P. Nordlander, "A hybridization model for the plasmon response of complex nanostructures," Science **302**, 419–422 (2003).
54. I. B. Udagedara, I. D. Rukhlenko, and M. Premaratne, "Complex-ω approach versus complex-k approach in description of gain-assisted surface plasmon-polariton propagation along linear chains of metallic nanospheres," Phys. Rev. B **83**, 115451 (2011).
55. I. B. Udagedara, I. D. Rukhlenko, and M. Premaratne, "Surface plasmon-polariton propagation in piecewise linear chains of composite nanospheres: The role of optical gain and chain layout," Opt. Express **19**, 19973–19986 (2011).
56. S. Link and M. A. El-Sayed, "Size and temperature dependence of the plasmon absorption of colloidal gold nanoparticles," J. Phys. Chem. B **103**, 4212–4217 (1999).
57. J. Li, G. Sun, and C. T. Chan, "Optical properties of photonic crystals composed of metal-coated spheres," Phys. Rev. B **73**, 075117 (2006).
58. D. D. Evanoff Jr. and G. Chumanov, "Size-controlled synthesis of nanoparticles. 2. Measurement of extinction, scattering, and absorption cross sections," J. Phys. Chem. B **108**, 13957–13962 (2004).
59. H. Trabelsi, M. Gantri, T. Sghaier, and E. Sediki, "Computational study of a possible improvement of cancer detection by diffuse optical tomography," Adv. Stud. Biol. **4**, 195–206 (2012).

#178972 - $15.00 USD Received 31 Oct 2012; revised 29 Nov 2012; accepted 29 Nov 2012; published 5 Dec 2012

60. A. M. Schwartzberg, T. Y. Olson, C. E. Talley, and J. Z. Zhang, "Synthesis, characterization, and tunable optical properties of hollow gold nanospheres," J. Phys. Chem. B **110**, 19935–19944 (2006).
61. E. D. Palik, *Handbook of Optical Constants of Solids* (Academic, Boston, 1985).

1. Introduction

Significant progress has been achieved over the past several decades in synthesizing high-quality metallic nanoparticles of different shapes and sizes [1]. Some of them—including nanoshells, nanorods, nanospheres, and nanocages made of gold—have been used as photothermal therapeutic agents for fighting cancers [2–9]. The destruction of cancerous cells benefits from the enhanced absorption of near-infrared (NIR) radiation by gold, due to the localized surface plasmon resonances of the nanoparticles, which make their extinction efficiencies several orders of magnitude larger than those of the conventional hyperthermia agents [6, 7]. Among various metallic nanoparticles, gold nanoshells are of particular importance, owing to their relatively simpler geometry and comparatively larger photothermal efficiency for equivalent number of nanoparticles [2, 10]. The biocompatibility and noncytotoxicity of gold enable them to be readily conjugated to antibodies or other biomolecules, in order to be delivered to the targeted malignant tumors [11]. The silica-based gold nanoshells have already been successfully used for the *in vitro*, as well as *in vivo*, plasmonic photothermal therapy (PPTT) aimed at brain, breast, liver, and prostate cancers [12–18].

The efficacy of gold nanoshells in PPTT depends on their dimensions, refractive indices of the core material and surrounding tissue, as well as on the spectrum of the excitation source [19–24]. Ample research efforts have thus been devoted to the analysis of these dependencies, with the intention to maximize the energy absorbed by nanoshells illuminated by a single-wavelength laser with peak wavelength typically ranging from 650 nm to 900 nm [3, 10, 25–29]. In particular, various optimization algorithms were employed to maximize the absorption efficiency of gold nanoshells embedded in specific types of cancerous tissue [25, 26]. Despite the fact that a wide variety of materials and excitation wavelengths were analyzed in these studies, a number of crucial questions on the optimization of gold nanoshells still need to be answered. First of all, it is not clear what would be the effect of broadband excitation on the absorption efficiency of the nanoshells and whether the use of broadband sources would benefit PPTT. The issue of broadband excitation is far from being trivial for two reasons: (i) real nanoshells are distributed in size, which leads to the inhomogeneous broadening of their absorption spectrum [11]; and (ii) there is always a compromise between the width of the excitation band and source intensity. By anticipating the use of broadband sources for cancer treatment, Zheng *et al.* [30] have recently demonstrated the therapeutic advantages of broadband visible and NIR emitters, where the carbon-nanotube-based nanostructures are used as the photothermal agents. Second, it is clear that the number of nanoshells that can be delivered to a particular tumor depends on their average size. Since the heat generation rate grows in proportion to this number, one needs to know the exact size dependency of the nanoshell density, in order to be able to find the optimal dimensions of the nanoshells that maximize the total energy absorbed in the tumor. Despite its obvious importance, the optimization problem allowing for the variation of nanoshell density with size has never been formulated so far, to the best of our knowledge. Third, it is often neglected in the optimization routines that gold nanoshells may scatter a significant amount of incident radiation, which may damage healthy tissue behind the targeted cancerous site. Meanwhile, the adverse effect of scattering is known to limit the usage of photothermal ablation therapy [6]. This indicates that maximization of the nanoshell absorption efficiency must be tackled not in isolation but by taking into account the scattering in the forward direction. The amount of forward scattering changes with the nanoshell's dimensions and is not the least when absorption peaks. This further complicates the optimization problem

#178972 - $15.00 USD Received 31 Oct 2012; revised 29 Nov 2012; accepted 29 Nov 2012; published 5 Dec 2012

and poses the challenge of finding the optimal dimensions for which gold nanoshells of a fixed absorption efficiency exhibit the lowest scattering. Finally, a number of issues are associated with modeling light propagation through a biological tissue [31]. Although the diffusion of light through tissue is well described by the photon transport equation [32, 33], it is still unclear how this equation has to be modified to take into account the effect of multiple scattering by the nanoshells. The effects of light diffusion and multiple scattering may be significant for the efficacy of PPTT at certain excitation wavelengths and when the nanoparticles are densely packed inside a tumor.

This paper presents the first study of absorption and scattering properties of a gold-nanoshell ensemble, taking into account the fact that the number of the nanoshells deliverable to a cancer site is a function of their size. We begin our study by formulating the general optimization problem for the ensemble of nanoshells with an arbitrary size distribution excited by a field of an arbitrary spectral density. The formulation is based on the exact analytical expressions for the absorption and scattering efficiencies of a composite nanoshell, and lays the foundation for the rapid calculation of optimal nanoshell parameters in any situation of practical interest. By considering the case of a sufficiently narrow size distribution and assuming the number of nanoshells to scale as $\propto R^{-\beta}$, where R is the mean nanoshell radius, we study the effect of β on the optimal nanoshell dimensions. The case of $\beta = 2$ is of particular heuristic and methodological interests, as it corresponds to the situation where the energy absorbed (scattered) by the ensemble becomes maximal for the same dimensions that maximize the absorption (scattering) efficiency of a single nanoshell. This situation is analyzed in detail by the example of silica-core gold nanoshells exposed to the radiation with a uniform spectrum between 650 and 900 nm. The optimal nanoshell radii are evaluated for all possible types of human tissues—with refractive indices ranging from 1.35 to 1.7—and the results are summarized in compact algebraic expressions, which can be further used without the need of performing numerical simulations. We also address the issue of minimizing the detrimental impact of PPTT on healthy tissue, by optimizing the nanoshell parameters to achieve the smallest possible scattering for a desired absorption efficiency.

2. Theoretical formulation

The interaction of nanoparticles with the incident electromagnetic field may be quantified in terms of their absorption and scattering efficiencies, Q_{abs} and Q_{sca}. These efficiencies depend on the size, shape, and composition of the nanoparticles. For the case of a gold nanoshell of inner radius R_1 and outer radius R_2, the absorption and scattering efficiencies at the wavelength λ are of the form [34]

$$Q_{\text{abs}}(R_1,R_2,\lambda) = \frac{1}{2}\left(\frac{\lambda}{\pi n_0 R_2}\right)^2 \sum_{n=1}^{\infty}(2n+1)\left[\text{Re}(a_n+b_n) - |a_n|^2 - |b_n|^2\right], \tag{1a}$$

$$Q_{\text{sca}}(R_1,R_2,\lambda) = \frac{1}{2}\left(\frac{\lambda}{\pi n_0 R_2}\right)^2 \sum_{n=1}^{\infty}(2n+1)\left(|a_n|^2 + |b_n|^2\right), \tag{1b}$$

where n_0 is the refractive index of the medium surrounding the nanoshell and a_n and b_n are the Mie scattering coefficients for a coated sphere. The Mie coefficients in Eq. (1) depend on the relative permittivity ε_1 of dielectric core and the relative permittivity $\varepsilon_2 = \varepsilon_2' + i\varepsilon_2''$ of gold coating (shell).

When the bandwidth of the incident field is sufficiently broad, it is the absorption and scattering energies accumulated over the entire field spectrum that are of major practical interest. By denoting $f(\lambda)$ the intensity spectral density of incident irradiation, the averaged absorption

#178972 - $15.00 USD Received 31 Oct 2012; revised 29 Nov 2012; accepted 29 Nov 2012; published 5 Dec 2012

and scattering efficiencies of the nanoshell can be defined as

$$S_{\rm abs}(R_1,R_2)=\int_0^\infty Q_{\rm abs}(R_1,R_2,\lambda)\,f(\lambda)\,{\rm d}\lambda, \tag{2a}$$

$$S_{\rm sca}(R_1,R_2)=\int_0^\infty Q_{\rm sca}(R_1,R_2,\lambda)\,f(\lambda)\,{\rm d}\lambda. \tag{2b}$$

If the spectral density is normalized by the condition

$$\int_0^\infty f(\lambda)\,{\rm d}\lambda=1, \tag{3}$$

then the quantities $P_{\rm abs}=\pi R_2^2 I_0 S_{\rm abs}$ and $P_{\rm sca}=\pi R_2^2 I_0 S_{\rm sca}$, with I_0 being the total intensity of the incident field, are the powers of absorption and scattering by the nanoshell.

The efficiencies of absorption and scattering by a nanoshell ensemble depend on the size distribution of the nanoshells. This distribution must be taken into account when one calculates the total powers $P^N_{\rm abs}$ and $P^N_{\rm sca}$ absorbed and scattered by the ensemble. It is common to optimize the efficacy of PPTT by neglecting the effects of multiple scattering by the nanoparticles and light diffusion through biological tissue [2,7,10–12,16,22,25,26,35]. This enables one to treat the nanoparticles independently, in which case the total heat generated by their ensemble is simply a sum of individual contributions. We also neglect the effects of excitation light coherence, the associated biological impact of light [36–38], and both the attenuation and scattering of light inside the human tissue [39]. With these assumptions, we may estimate $P^N_{\rm abs}$ and $P^N_{\rm sca}$ by averaging the absorption and scattering powers of a single nanoshell over the distribution $g(R_1,R_2,\bar{R}_1,\bar{R}_2)$,

$$P^N_{\rm abs}(\bar{R}_1,\bar{R}_2)=\int_0^\infty\int_0^\infty P_{\rm abs}(R_1,R_2,\lambda)\,g(R_1,R_2,\bar{R}_1,\bar{R}_2)\,{\rm d}R_1{\rm d}R_2, \tag{4a}$$

$$P^N_{\rm sca}(\bar{R}_1,\bar{R}_2)=\int_0^\infty\int_0^\infty P_{\rm sca}(R_1,R_2,\lambda)\,g(R_1,R_2,\bar{R}_1,\bar{R}_2)\,{\rm d}R_1{\rm d}R_2, \tag{4b}$$

where $\bar{R}_1$ and $\bar{R}_2$ are the mean radii and the function $g(R_1,R_2,\bar{R}_1,\bar{R}_2)$ is normalized to the total number N of the nanoshells in the ensemble, i.e.,

$$\int_0^\infty\int_0^\infty g(R_1,R_2,\bar{R}_1,\bar{R}_2)\,{\rm d}R_1{\rm d}R_2=N(\bar{R}_1,\bar{R}_2). \tag{5}$$

The number of the nanoshells in a tumor of given volume V can, in principle, be a function of both $\bar{R}_1$ and $\bar{R}_2$. However, it is often the outer radius that determines the average nanoshell density $\rho(\bar{R}_2)=N(\bar{R}_2)/V$ in the tumor. Despite the fact that the efficacy of PPTT strongly depends on the nanoshell density, its impact on the optimal design of gold nanoshells has never been considered so far, to the best of our knowledge.

In order to maximize (minimize) the energy absorbed (scattered) over a given period of time by the nanoshell ensemble with a fixed $\bar{R}_2$, one needs to maximize (minimize) the averaged total power $P^N_{\rm abs}$ ($P^N_{\rm sca}$) given in Eq. (4), by varying the average thickness of the gold coating. Numerical simulations show that the optimal nanoshells may be as thin as a few nanometers [2, 21,25]. Since such thicknesses are much smaller than the mean free path of conduction electrons in bulk gold, which is about 42 nm at room temperature [40], one needs to take into account the increased ohmic losses due to the higher collision rate of electrons [23, 24, 41]. This can be done by modifying the permittivity $\varepsilon_2(\omega)$ [42] of bulk gold as follows:

$$\varepsilon_2(R_1,R_2,\omega)=\varepsilon_2(\omega)+\frac{\omega_p^2}{\omega^2+i\omega\gamma}-\frac{\omega_p^2}{\omega^2+i\omega\Gamma(R_1,R_2)}, \tag{6}$$

#178972 - $15.00 USD Received 31 Oct 2012; revised 29 Nov 2012; accepted 29 Nov 2012; published 5 Dec 2012

where $\omega_p = 1.36 \times 10^{16}$ rad/s, $\gamma = 1.05 \times 10^{14}$ rad/s, $\Gamma(R_2, R_1) = \gamma + v_F/(R_2 - R_1)$, and $v_F = 1.4 \times 10^6$ m/s is the Fermi velocity. The last two terms in this expression allow for the change $\delta\varepsilon_2$ in the permittivity resulting from the increased collision rate, which tends to zero with shell thickness as $\delta\varepsilon_2 \propto 1/(R_2 - R_1)$.

3. Effect of number density on optimal design of gold nanoshells

The theory presented in the previous section enables us to analyze how the efficacy of PPTT varies with the number of gold nanoshells. This efficacy is determined by the total powers P^N_{abs} and P^N_{sca}, which depend on $\bar{R}_1$, $\bar{R}_2$, $\rho(\bar{R}_2)$, $f(\lambda)$, and the size distribution $g(R_1, R_2, \bar{R}_1, \bar{R}_2)$. For given functions $\rho(\bar{R}_2)$, $f(\lambda)$, and $g(R_1, R_2, \bar{R}_1, \bar{R}_2)$, it is always possible to find the optimal nanoshell radii, $\bar{R}_1^{\text{opt}}$ and $\bar{R}_2^{\text{opt}}$, which ensure that the photothermal therapy is the most efficient under the circumstances. On the other hand, for a given size and spectral distributions, the optimal radii are determined by the nanoshell number density $\rho(\bar{R}_2)$.

We study the effect of number density on the optimal dimensions of the nanoshell for the situation where the intensity of the incident field is almost uniform across the spectral range from λ_1 to λ_2, in which case

$$f(\lambda) = \frac{H(\lambda - \lambda_1) - H(\lambda - \lambda_2)}{\lambda_2 - \lambda_1}, \tag{7}$$

where $H(\lambda)$ is the Heaviside step function. The uniform intensity distribution can be achieved either using broadband near-infrared emitters, like superluminescent and broadband laser diodes [43–46] in stand-alone or array configuration, or spectrally shaping supercontinuum laser sources [47]. The boundary wavelengths λ_1 and λ_2 are usually determined by the transparency window of biological tissue or the pass-band of optical filters.

Without loss of generality, we also assume that nearly identical nanoshells of mean radii $\bar{R}_1$ and $\bar{R}_2$ are delivered to the cancerous tissue, and that their number in a fixed volume of the tissue is inversely proportional to their size. This situation may be described by the distribution

$$g(R_1, R_2, \bar{R}_1, \bar{R}_2) = A\bar{R}_2^{-\beta}\delta(R_1 - \bar{R}_1)\delta(R_2 - \bar{R}_2), \tag{8}$$

where A is a constant of dimensionality $[L]^\beta$, $\beta > 0$ is the density index, and δ is the Dirac's δ-function. Using this distribution in Eq. (4), we obtain

$$P^N_{\text{abs}}(\bar{R}_1, \bar{R}_2) = \pi A I_0 \bar{R}_2^{2-\beta} S_{\text{abs}}(\bar{R}_1, \bar{R}_2), \quad P^N_{\text{sca}}(\bar{R}_1, \bar{R}_2) = \pi A I_0 \bar{R}_2^{2-\beta} S_{\text{sca}}(\bar{R}_1, \bar{R}_2). \tag{9}$$

The value of β can be found provided the average nanoshell radii $\bar{R}_2^{(a)}$ and $\bar{R}_2^{(b)}$ are known for two colloidal solutions of densities $\rho^{(a)}$ and $\rho^{(b)}$, and is given by the expression

$$\beta = \frac{\ln\left(\rho^{(a)}/\rho^{(b)}\right)}{\ln\left(\bar{R}_2^{(b)}/\bar{R}_2^{(a)}\right)}. \tag{10}$$

It is seen from Eq. (9) that the optimal dimensions of gold nanoshell depend critically on the density index β, which shows how steeply the nanoshells' concentration decays with their size. For example, the values $\beta = 1$, 2, and 3 correspond to the situations where the number of nanoshells inside the cancerous tissue decreases in proportion to their average diameter, surface area, and volume, respectively. We illustrate this dependency by calculating P^N_{abs} and P^N_{sca} for the spectral window from 650 to 900 nm [3, 4]. The inner and outer radii are considered in the domain of 1 nm $\leq \bar{R}_1 < \bar{R}_2 \leq$ 200 nm, which covers the entire range of nanoshells suitable for PPTT [48] (hereinafter, for the sake of simplicity, we omit the bar symbols above the mean nanoshell radii).

#178972 - $15.00 USD Received 31 Oct 2012; revised 29 Nov 2012; accepted 29 Nov 2012; published 5 Dec 2012

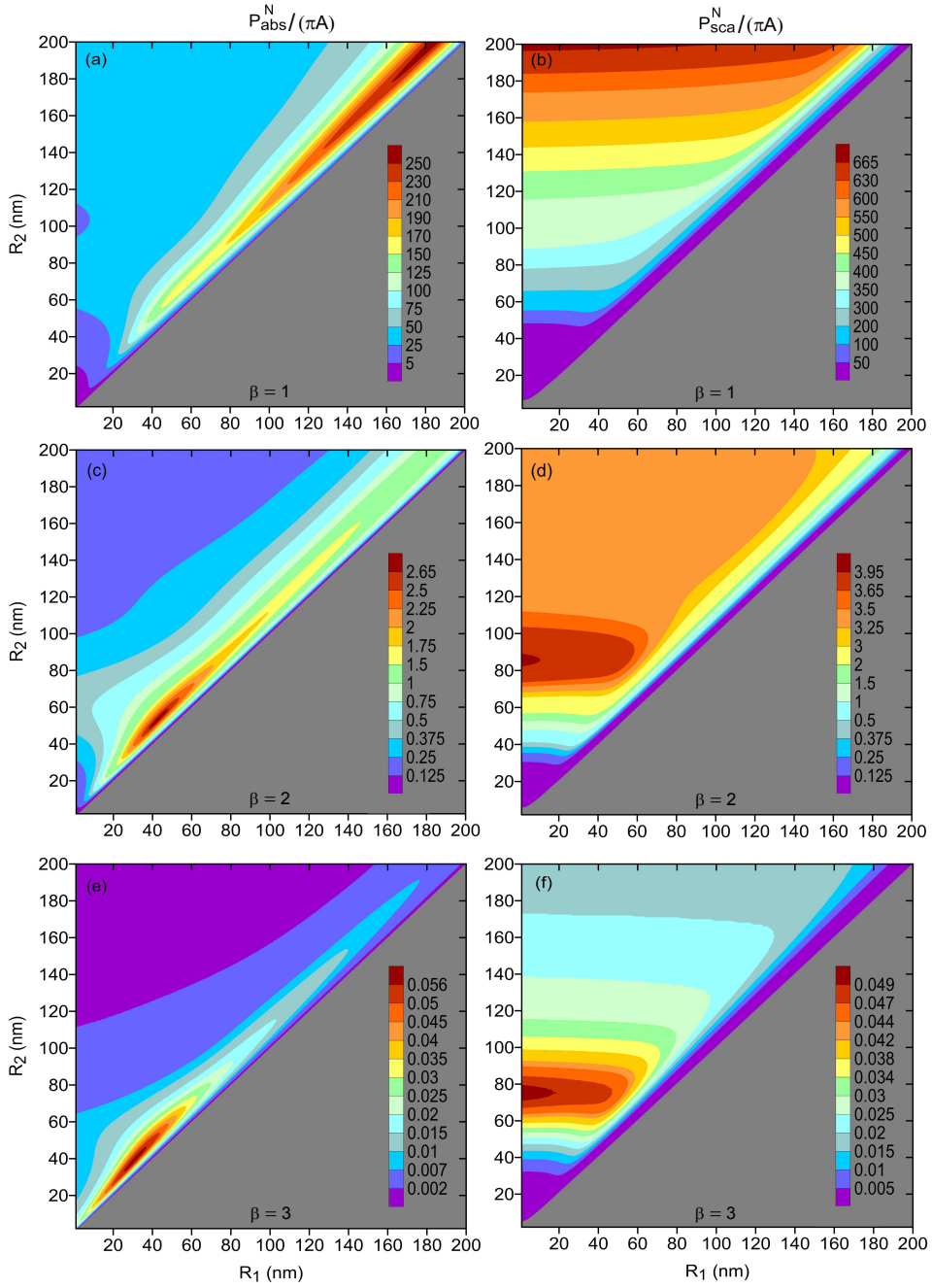

Fig. 1. Normalized average powers absorbed (left panels) and scattered (right panels) by three Si@Au nanoshell ensembles. The total number N of the nanoshells in the ensembles vary as $N(R_2) \propto R_2^{-\beta}$, where $\beta = 1$ in (a) and (b), $\beta = 2$ in (c) and (d), and $\beta = 3$ in (e) and (f). In all cases, nanoshells were assumed to be embedded in cancerous tissue with $n_0 = 1.44$; the refractive index of silica was taken from Ref. [49].

#178972 - $15.00 USD Received 31 Oct 2012; revised 29 Nov 2012; accepted 29 Nov 2012; published 5 Dec 2012

Figure 1 shows the normalized powers absorbed and scattered by the nanoshell ensemble for three types of size dependencies of the nanoshell density—corresponding to the indices $\beta = 1$, 2, and 3. It is assumed that the nanoshells are surrounded by a medium of refractive index 1.44 and their cores are made of silica, whose permittivity is described by the Sellmeier equation from Ref. [49]. One can see that the nanoshell radii corresponding to the maxima of the absorbed and scattered powers depend critically on how the nanoshell density vary with the nanoshell size. When $\beta = 1$ and $\rho \propto 1/R_2$ [see Figs. 1(a) and 1(b)], the strongest absorption and scattering occur for the nanoshells of diameters 400 nm, i.e., at the edge of the parametric domain of interest (absorption peaks for $R_1 \approx 180$ nm, while scattering becomes maximal for pure gold nanoshells). Unfortunately, it is not feasible to use such large nanoshells in photothermal therapy, as they exceed the maximal diameter of the capillaries surrounding the tissue and cannot be efficiently delivered to tumors [48]. In this situation, the optimal nanoshell radii R_2^{opt} is to be selected as large as possible, while ensuring that the nanoshells can reach the targeted site. The optimal inner radius is then given by $R_1^{\text{opt}} \approx 0.9427 R_2^{\text{opt}} - 5.79$ (here, both R_1 and R_2 are in nanometers).

When $\rho \propto 1/R_2^2$ or $\propto 1/R_2^3$, which is illustrated by Figs. 1(c)–1(f), the optimal nanoshell diameters fall within the range 80–110 nm. It is seen that the steeper the nanoshell density decreases with R_2, the smaller the optimal nanoshell diameters are. This result is intuitively clear, since total absorption (scattering) cross section of the ensemble starts to benefit less from large absorption (scattering) cross sections of big nanoshells, due to their reduced numbers. The comparison of Figs. 1(a), 1(c), and 1(e) also shows that the optimal nanoshell radii are most sensitive to small values of β and change drastically when $\beta \lesssim 1$. Notice that the case of $\beta = 0$ (not shown) corresponds to the hypothetical situation when the density of the nanoshells inside a tumor is independent of their size.

It should be recognized that the function $N(R_2) = AR_2^{-\beta}$ cannot coincide with the real dependency of the nanoshell number on size in the entire range of R_2. The reason is that the small nanoshells (with $R_2 < 10$ nm) penetrate the cells and easily diffuse out of the cancerous tissue. Therefore, the actual function $N(R_2)$ rather grows for small R_2, due to the increase in the number of nanoshell accumulated inside the tumor with their size, and starts to decay later when the nanoshell size exceeds the capillary diameter. For example, in real ensembles with broad size distribution of the nanoshells, both the outer nanoshell radius and shell thickness $h = R_2 - R_1$ are typically distributed according to the lognormal function [50], in which case

$$g(R_2, h, \mu_{R_2}, \sigma_{R_2}, \mu_h, \sigma_h) = \frac{N}{2\pi R_2 h \sigma_{R_2} \sigma_h} \exp\left(- \frac{\left(\ln R_2 - \mu_{R_2}\right)^2}{2\sigma_{R_2}^2} - \frac{\left(\ln h - \mu_h\right)^2}{2\sigma_h^2} \right),$$

where μ_{R_2} and σ_{R_2} are the mean and standard deviations of $\ln R_2$, and μ_h and σ_h are the mean and standard deviations of $\ln h$. The fact that the function $N(R_2)$ we used is only an approximation to the real dependency does not alter the qualitative results of this section, which indicates that the number density of gold nanoshells is crucial for the efficacy optimization of PPTT. These results would also hold true, should we consider a different spectrum of excitation source or allow for a broad size distribution of the nanoshells.

4. Optimal design of gold nanoshells for $\beta = 2$

In order to explain the origin of maxima in Fig. 1 and estimate the optimal design of gold nanoshells for different therapeutic usages, we now focus on the situation where the density of the nanoshells is inversely proportional to their cross section area. This situation is of particular interest, as the energies absorbed and scattered by the nanoshell ensemble in this case are determined solely by the average efficiencies S_{abs} and S_{sca} of a nanoshell. As before, we evaluate

#178972 - $15.00 USD Received 31 Oct 2012; revised 29 Nov 2012; accepted 29 Nov 2012; published 5 Dec 2012

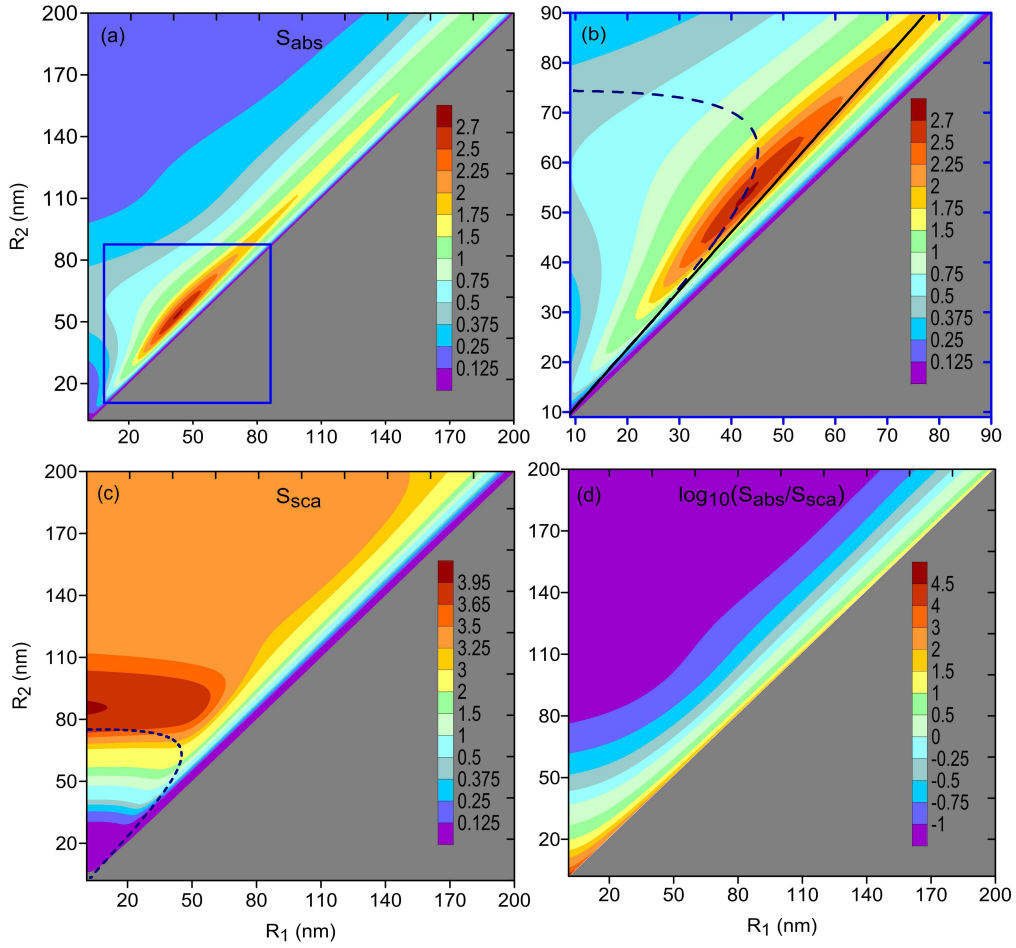

Fig. 2. Average [(a) and (b)] absorption and (c) scattering efficiencies of gold nanoshells with silica core [(b) is the magnified part of (a)]; the nanoshells were assumed to be surrounded by cancerous tissue with $n_0 = 1.44$. Solid line (of slope 1.17) and dashed curve show the optimal nanoshell dimensions predicted with the quasistatic approximation using Eqs. (11) and (13), respectively. (d) Ratio of average absorption efficiency to average scattering efficiency in logarithmic scale. Density index $\beta = 2$ in all cases.

the optimal dimensions of gold nanoshells for broadband near-infrared excitation, by setting $\lambda_1 = 650$ nm and $\lambda_2 = 900$ nm. Since it is required to treat cancer in different parts of human body, the design of the nanoshells significantly varies depending on the type of the cancerous tissue. The optimal nanoshell radii are tailored to particular situations by considering different refractive indices of the cancerous tissue and different dielectric fillings of the core.

4.1. SiO_2@Au nanoshells

We first consider the case where gold nanoshells with silica core (SiO_2@Au nanoshells) are delivered to the cancerous subcutaneous adipose tissue (fat). At the preliminary growth stage of cancer, this tissue is characterized by the refractive index $n_0 = 1.44$ [51, 52]. Figures 2(a)–2(c) show the average absorption and scattering efficiencies in the (R_1, R_2) domain. It is seen

#178972 - $15.00 USD Received 31 Oct 2012; revised 29 Nov 2012; accepted 29 Nov 2012; published 5 Dec 2012

that $S_{\rm abs}$ peaks for $R_1 \approx 42.5$ nm and $R_2 \approx 53$ nm (with a value of about 2.7), while $S_{\rm sca}$ has its maximum (of about 4) for a solid gold nanosphere of radius around 85 nm.

The origin of the peak in Fig. 2(a) can be understood with the plasmon hybridization theory [53]. According to this theory, a gold nanoshell supports two surface plasmon modes, with symmetric and antisymmetric charge distributions on the inner and outer metal–dielectric interfaces. The two modes merge into a single surface plasmon resonance centered at $\lambda \approx 520$ nm when the dielectric core shrinks and the nanoshell transforms into a pure gold nanosphere. On the other hand, as the core expands, the low-frequency symmetric mode shifts towards larger wavelengths, while the high-frequency antisymmetric mode exhibits a blue shift. It is therefore reasonable to expect the highest absorption efficiency for those nanoshells whose symmetric plasmon mode is located near the center wavelength $\lambda_c = (\lambda_1 + \lambda_2)/2 = 775$ nm.

The ratio $x = R_1/R_2$ for the peak may be readily estimated using the quasistatic approximation. Within the frame of this approximation, the nanoshell is represented by an electric dipole of polarizability [34]

$$\alpha = \frac{\varepsilon_2\varepsilon_a - \varepsilon_3\varepsilon_b}{\varepsilon_2\varepsilon_a + 2\varepsilon_3\varepsilon_b} R_2^3, \tag{11}$$

where $\varepsilon_a = \varepsilon_1(1+2x^3) + 2\varepsilon_2(1-x^3)$, $\varepsilon_b = \varepsilon_1(1-x^3) + \varepsilon_2(2+x^3)$, and $\varepsilon_3 = n_0^2$. The polarizability peaks at λ_c for those nanoshells that satisfy the resonance condition $\mathrm{Re}(\varepsilon_2\varepsilon_a + 2\varepsilon_3\varepsilon_b) = 0$, which may be rewritten as [23, 54, 55]

$$x^3 = 1 + \frac{3\varepsilon_2'(\varepsilon_3 + \varepsilon_1/2)}{(\varepsilon_2')^2 - (\varepsilon_2'')^2 - \varepsilon_2'(\varepsilon_1 + \varepsilon_3) + \varepsilon_1\varepsilon_3}. \tag{12}$$

For $\lambda_c = 775$ nm, this expression gives $x \approx 0.85$. The optimal dimensions of gold nanoshell predicted in this way are shown in Fig. 2(b) by the solid line. Although this line slightly misses the exact peak of the average absorption efficiency (corresponding to $x \approx 0.8$), it still closely follows the ridge of the function $S_{\rm abs}(R_1, R_2)$. This mismatch is due to the fact that the quasistatic approximation in Eq. (11) is not equally accurate over the entire range of nanoshell sizes being considered. The extinction cross sections of small gold nanoshells (with diameters less than 25 nm) are dominated by the dipolar contribution. However, as the nanoshells become larger, the higher-order plasmon modes (quadrupole, octupole, *etc.*) start to noticeably contribute the extinction and the quasistatic approximation becomes inapplicable [56].

In order to be able to estimate the position of the scattering efficiency maximum, one should take into account the reduction in the depolarization field inside the nanoshell core due to the decrease in the coherence of plasma oscillations with R_2 (resulting in a red shift of the plasmon resonance), and the radiation damping (leading to spectral broadening of the plasmon resonance). With these corrections, the modified polarizability is of the form [57]

$$\hat{\alpha} = \frac{\alpha}{1 - \alpha k_3^2/R_2 - (2i/3)\alpha k_3^3}, \tag{13}$$

where α is given in Eq. (7) and $k_3 = 2\pi n_0/\lambda$. The polarizability $\hat{\alpha}$ peaks when R_1 and R_2 satisfy the equation $(k_3^2/R_2)\,\mathrm{Re}\,\alpha = 1 + (2/3)\,k_3^3\,\mathrm{Im}\,\alpha$. The resonance dependency $R_2(R_1)$ given by this equation for $\lambda_c = 775$ nm is shown by the dashed curve in Figs. 2(b) and 2(c). The curve approximately corresponds to the nanoshell dimensions that result in the local maxima of the averaged extinction efficiency, $S_{\rm ext} = S_{\rm abs} + S_{\rm sca}$. The relative contributions of absorption and scattering to the extinction vary along the curve $R_2(R_1)$. Absorption dominates over scattering in thin nanoshells with $R_2 < 62$ nm, due to the steep growth of ohmic losses with the reduction in shell thickness. For larger R_2, scattering exceeds absorption, owing to the increased effect

#178972 - $15.00 USD Received 31 Oct 2012; revised 29 Nov 2012; accepted 29 Nov 2012; published 5 Dec 2012

of dynamic depolarization and radiative damping [22, 57, 58]. Hence, the resonance curve in Figs. 2(b) and 2(c) indicates the approximate positions of the local maxima of the function $S_{\rm abs}(R_1,R_2)$ when $R_2 < 62$ nm, and those of the function $S_{\rm sca}(R_1,R_2)$ when $R_2 \geqslant 62$ nm.

Generally, the refractive index of a healthy tissue in a human body falls within the range 1.35 to 1.55 [52]. When a tissue gets cancerous, its refractive index may increase up to 10% as compared to that of the healthy one [59]. We calculate the optimal dimensions $R_1^{\rm opt}$ and $R_2^{\rm opt}$ maximizing the absorption efficiency of gold nanoshells for all types of cancerous tissues at their different growth stages, by varying n_0 from 1.35 to 1.7. The obtained data is then used to express the optimal dimensions as functions of the refractive index of the cancerous tissue, with the result

$$R_1^{\rm opt} \approx 35n_0^2 - 149n_0 + 185, \tag{14a}$$

$$R_2^{\rm opt} \approx 40n_0^2 - 165n_0 + 208. \tag{14b}$$

These expressions give the optimal values of R_1 and R_2 (in nanometers) with accuracy of ± 0.5 nm for $n_0 \in [1.35, 1.7]$.

4.2. Minimizing adverse effects of PPTT with SiO_2@Au nanoshells

To ensure that minimal thermal injury is caused by PPTT to the healthy cells surrounding the malignant tumor, one needs to minimize the scattering by the nanoshells. For a given absorption efficiency, this can be achieved by maximizing the ratio $S_{\rm abs}/S_{\rm sca}$ shown in Fig. 2(d). It is seen that this ratio grows with the reduction either in shell thickness (for a fixed R_2) or the size of the nanoshell (for a fixed R_1). Unfortunately, neither nanoshells with relatively thin coatings (such that $R_2 - R_1 \ll R_2$), nor small nanoshells (with $R_2 \lesssim 18$ nm) absorb significantly in the spectral range of interest, as is evident from Figs. 2(a) and 2(b). Moreover, the small nanoshells may easily diffuse out of the tumor and are useless for the purposes of PPTT [60]. This poses the problem of finding the dimensions of the nanoshells that exhibit the least scattering for any absorption efficiency exceeding a desired threshold value $S_{\rm abs}^{\rm (th)}$, which is dictated by the tolerable radiation exposure time.

Figures 3(a) and 3(b) show how the minimal value of $S_{\rm sca}$ and the maximal value of $S_{\rm abs}/S_{\rm sca}$ vary with the refractive index n_0 for SiO_2@Au nanoshells with $S_{\rm abs} \geq S_{\rm abs}^{\rm (th)} = 1$, 1.5, 2, and 2.5. One can see that the scattering is minimal for $S_{\rm abs}^{\rm (th)} = 1.0$ and rises with the threshold absorption efficiency regardless of n_0. An opposite trend is observed for the ratio $S_{\rm abs}/S_{\rm sca}$; it decays with $S_{\rm abs}^{\rm (th)}$ and attains its minimal values when $S_{\rm abs}^{\rm (th)} = 2.5$. Of significance from the application viewpoint is that $S_{\rm sca}$ decays, while $S_{\rm abs}/S_{\rm sca}$ grows, with the refractive index of the cancerous tissue. This feature makes SiO_2@Au nanoshells more efficient in treating cancer at its final growth stages. Also noteworthy is that the absorption efficiencies corresponding to the minimal $S_{\rm sca}$ in Fig. 3(a) approximately equal to the respective thresholds.

The optimal dimensions $R_1^{\rm opt}$ and $R_2^{\rm opt}$, which correspond to the minimal scattering efficiencies in Fig. 3(a), are shown in Figs. 3(c) and 3(d). The scattering by the largest nanoshells (corresponding to $S_{\rm abs}^{\rm (th)} = 2.5$) is seen to cause the worst thermal injury, which severely limits the applicability of such nanoshells in PPTT. The optimal dimensions (in nanometers) for the

#178972 - $15.00 USD Received 31 Oct 2012; revised 29 Nov 2012; accepted 29 Nov 2012; published 5 Dec 2012

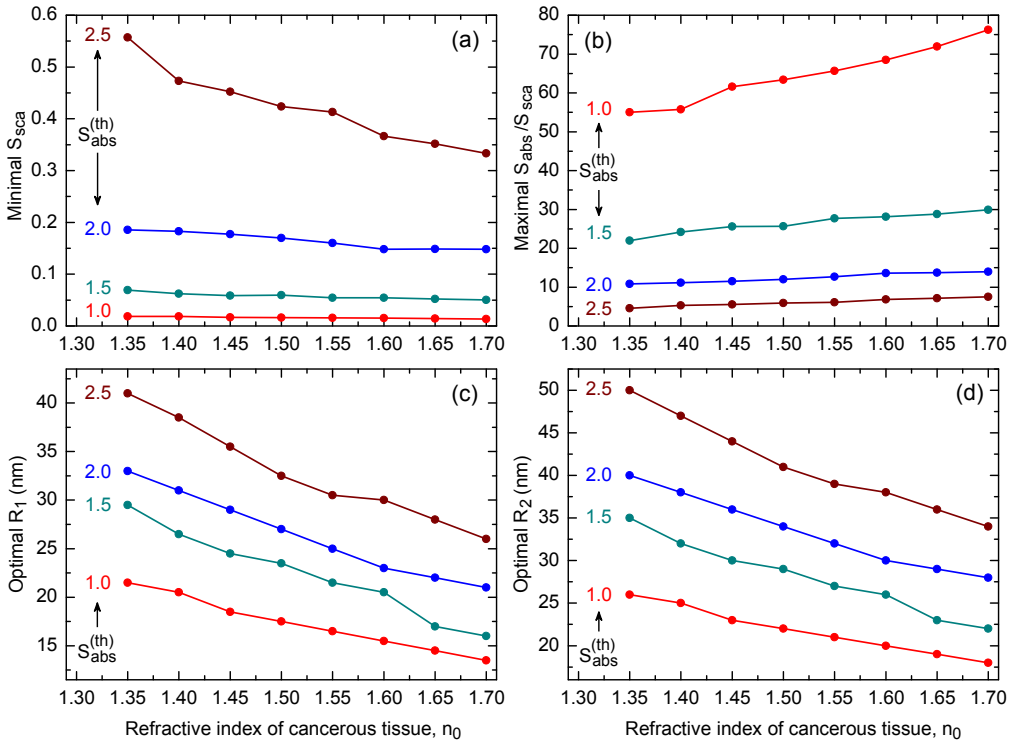

Fig. 3. Variation of (a) minimal $S_{\rm sca}$, (b) maximal $S_{\rm abs}/S_{\rm sca}$, (c) optimal R_1, and (d) optimal R_2 with refractive index of cancerous tissue for different absorption thresholds $S_{\rm abs}^{\rm (th)}$ of SiO_2@Au nanoshell. The exact values are shown by filled circles, which are joined together by lines serving as guides for eyes.

remaining thresholds may be approximated by the expressions

$$R_1^{\rm opt} \approx \begin{cases} 19n_0^2 - 81n_0 + 96 & \text{for } S_{\rm abs}^{\rm (th)} = 1, \\ 14n_0^2 - 79n_0 + 110 & \text{for } S_{\rm abs}^{\rm (th)} = 1.5, \\ 36n_0^2 - 144n_0 + 162 & \text{for } S_{\rm abs}^{\rm (th)} = 2, \end{cases} \tag{15a}$$

$$R_2^{\rm opt} \approx R_1^{\rm opt} + \begin{cases} 5 & \text{for } S_{\rm abs}^{\rm (th)} = 1, \\ 6 & \text{for } S_{\rm abs}^{\rm (th)} = 1.5, \\ 7 & \text{for } S_{\rm abs}^{\rm (th)} = 2, \end{cases} \tag{15b}$$

with accuracy of about ± 0.5 nm for $n_0 \in [1.35, 1.7]$.

4.3. Effect of core material on PPTT efficiency

The permittivity of core material is one of the key factors that affect the position and intensity of the plasmon resonance [34]. By changing this material, one may further improve the performance of gold nanoshells in terms of their absorption and scattering efficiencies. This may be seen from Fig. 4, where these efficiencies are shown for gold nanoshells filled with silicon ($n_1 \approx 3.5$), silica ($n_1 \approx 1.4$), and air ($n_1 = 1$). The comparison of Figs. 4(a), 4(c), and 4(e) indicates that the optimal shell thickness increases, and the peak value of $S_{\rm abs}$ reduces,

#178972 - $15.00 USD Received 31 Oct 2012; revised 29 Nov 2012; accepted 29 Nov 2012; published 5 Dec 2012

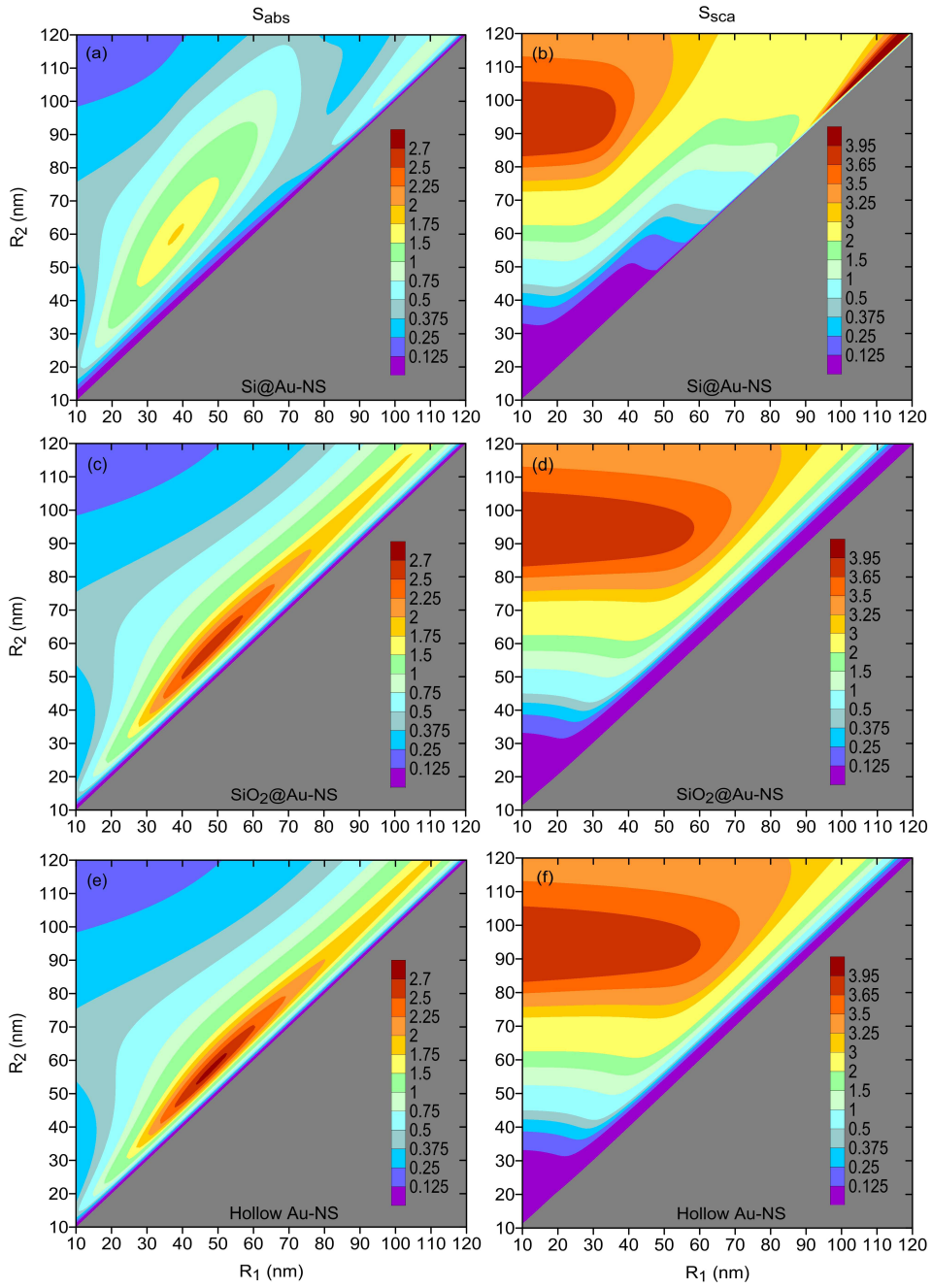

Fig. 4. Average absorption (left panels) and scattering (right panels) efficiencies of [(a) and (b)] Si@Au nanoshells, [(c) and (d)] SiO_2@Au nanoshells, and [(e) and (f)] hollow gold nanoshells. The nanoshells were assumed to be embedded in cancerous tissue with $n_0 = 1.35$; the refractive index of silicon was taken from Ref. [61].

#178972 - $15.00 USD Received 31 Oct 2012; revised 29 Nov 2012; accepted 29 Nov 2012; published 5 Dec 2012

as the refractive index of the core becomes larger. Since the scattering efficiencies of hollow nanoshells and SiO_2@Au nanoshells are almost the same [see Figs. 4(d) and 4(f)], hollow nanoshells provide the highest absorption-to-scattering ratio and cause the least damage to the healthy neighboring tissue. Given that these nanoshells may be fabricated more precisely than the nanoshells filled with high-index dielectrics [19, 20], they deserved to be analyzed further.

Optimization of hollow nanoshells is performed similarly to how it was done in Section 4.1. As before, we focus on the situations where the preset radiation exposure time demands the absorption efficiency to exceed one of the four threshold values: 1.0, 1.5, 2.0, or 2.5. The results of the optimization run for cancerous tissues of refractive indices 1.35, 1.45, and 1.55 are presented in Table 1. For reference, the same table also includes the data for gold nanoshells filled with silica. The optimal ratio $S_{\rm abs}/S_{\rm sca}$ is seen to be larger for hollow nanoshells and to grow with the refractive index of the surrounding tissue. This is a consequence of the fact that the coatings of hollow nanoshells are slightly thinner than the coatings of SiO_2@Au nanoshells.

The variation of minimal $S_{\rm sca}$, maximal $S_{\rm abs}/S_{\rm sca}$, and the optimal dimensions of hollow gold nanoshells with n_0 is shown in Fig. 5. It is evident from Figs. 5(a) and 5(b) that the treatment of malignant tumors with nanoshells of lower absorption efficiencies over longer durations is less harmful to the surrounding healthy tissue than that with strongly absorbing nanoshells irradiated over shorter periods (provided that the radiation exposure time is much smaller than the heat dissipation constant).

The optimal core and shell radii as functions of $n_0 \in [1.35, 1.7]$ are shown in Figs. 5(c) and 5(d). The polynomial fittings to these functions (with accuracy of about ± 0.5 nm) are found to be given by

$$R_1^{\rm opt} \approx \begin{cases} 19n_0^2 - 75n_0 + 87 & \text{for } S_{\rm abs}^{\rm (th)} = 1, \\ 19n_0^2 - 81n_0 + 101 & \text{for } S_{\rm abs}^{\rm (th)} = 1.5, \\ 29n_0^2 - 116n_0 + 136 & \text{for } S_{\rm abs}^{\rm (th)} = 2, \end{cases} \tag{16a}$$

$$R_2^{\rm opt} \approx R_1^{\rm opt} + \begin{cases} 4 & \text{for } S_{\rm abs}^{\rm (th)} = 1, \\ 5 & \text{for } S_{\rm abs}^{\rm (th)} = 1.5, \\ 6 & \text{for } S_{\rm abs}^{\rm (th)} = 2. \end{cases} \tag{16b}$$

Since Eqs. (14) to (16) are derived based on the exact solution to the Maxwell's equations

Table 1. Optimal dimensions of gold nanoshells for three types of cancerous tissues and two types of core material. The values of ratio $S_{\rm abs}/S_{\rm sca}$ are rounded up to one decimal point. For more detail, see Fig. 5.

		Hollow gold nanoshell			SiO_2@Au nanoshell		
n_0	$S_{\rm abs}^{\rm (th)}$	$R_1^{\rm opt}$(nm)	$R_2^{\rm opt}$(nm)	$S_{\rm abs}/S_{\rm sca}$	$R_1^{\rm opt}$(nm)	$R_2^{\rm opt}$(nm)	$S_{\rm abs}/S_{\rm sca}$
1.35	1.0	20	24	66.3	21.5	26	55.0
	1.5	26	31	26.2	29.5	35	22.0
	2.0	32	38	12.6	33	40	10.8
	2.5	38.5	46	5.8	41	50	4.5
1.45	1.0	18	22	70.6	18.5	23	61.6
	1.5	23	28	28.6	24.5	30	25.6
	2.0	29	35	13.1	29	36	11.5
	2.5	33.5	41	6.5	35.5	44	5.6
1.55	1.0	16	20	77.2	16.5	21	65.7
	1.5	21	26	29.8	21.5	27	27.7
	2.0	25	31	15.0	25	32	12.7
	2.5	29.5	37	7.1	30.5	39	6.1

#178972 - $15.00 USD Received 31 Oct 2012; revised 29 Nov 2012; accepted 29 Nov 2012; published 5 Dec 2012

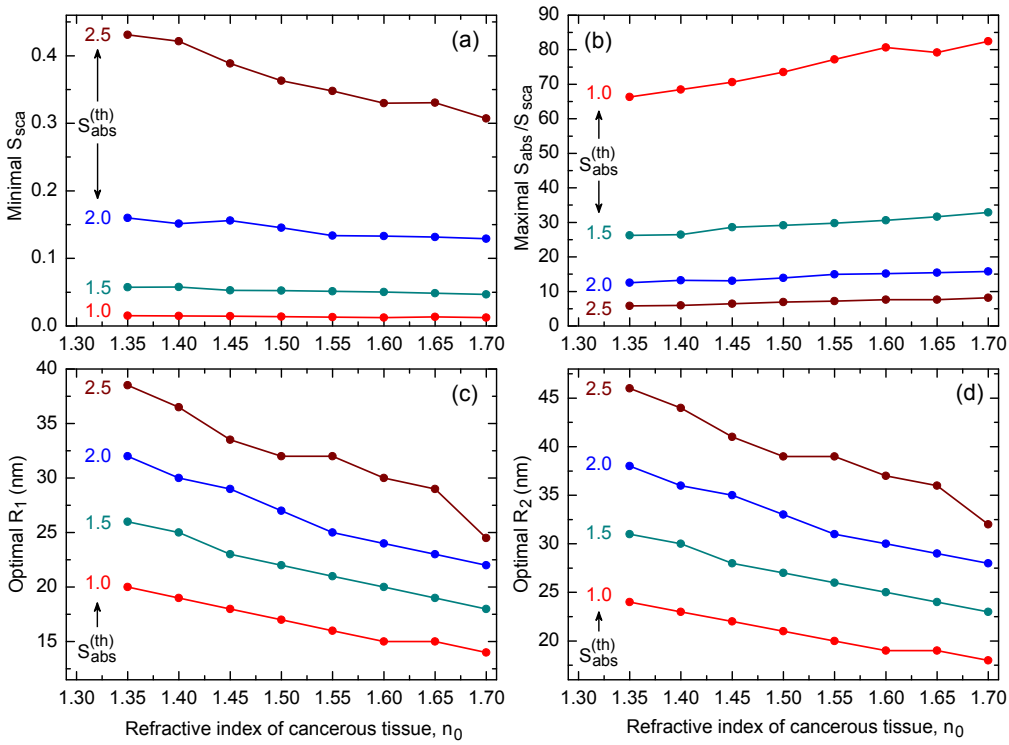

Fig. 5. Same as in Fig. 3 for hollow gold nanoshells. The exact values shown by filled circles are joined together by lines serving as guides for eyes.

and take into account the actual dispersion properties of the nanoshell constituents, the design parameters provided by them may be directly implemented in practice.

The accuracy of the optimal radii calculated with Eqs. (14)–(16) depends on the precision of n_0. If n_0 is known exactly, then the numerical values of the optimal nanoshell radii should be rounded according to the limitations of the fabrication process. Hollow nanoshells can be currently synthesized with a precision of 0.6 nm, whereas metal-dielectric nanoshells suffer from lower precision of about 1 to 2 nm [25,26]. The minor inaccuracies of fabrication of nanoshells can be tolerated, owing to the relative broadness of the absorption peaks. For example, the absorption peak in Fig. 4(e) shows that absorption efficiency exceeding 90% of its peak value can be attained for $R_1 = (48 \pm 4)$ nm and $R_2 = (57 \pm 4.5)$ nm. It should be also noted that the tolerance of the optimal nanoshell radii to the refractive index of the surrounding tissue varies with the absorption threshold and can be readily estimated using Eqs. (15) and (16).

5. Conclusions

Recently, gold nanoshells have become widely used as photothermal therapeutic agents for cancer treatment, due to their strong localized surface plasmon resonances. Such nanoshells can absorb infrared radiation much more efficiently than typical hyperthermia agents do, and are capable of generating heat that is sufficient for destroying the adjoining cancerous tissue. In this paper, we have studied the effect of the nanoshell number density on the absorption and scattering efficiencies of single-core gold nanoshells illuminated by broadband near-infrared light. By assuming that the number of the nanoshells delivered at a tumor site decreases with

#178972 - $15.00 USD Received 31 Oct 2012; revised 29 Nov 2012; accepted 29 Nov 2012; published 5 Dec 2012

their mean radius as $\propto R^{-\beta}$, we showed that the optimal nanoshell dimensions depend critically on β. It was found that the energy absorbed (scattered) by the ensemble with $\beta = 2$ reaches its maximum for the same dimensions with which an individual nanoshell exhibits the maximum absorption (scattering) efficiency. The special case of $\beta = 2$ was examined in detail for gold nanoshells with silica core. In particular, by considering a wide range of human tissues, we calculated the optimal inner and outer radii that maximize nanoshell absorption, and the radii that minimize nanoshell scattering for a fixed absorption efficiency. The obtained results allow one to reduce the detrimental impact of heat on healthy tissue around the targeted cancer site. By comparing gold nanoshells of different dielectric fillings, we found that hollow nanoshells of low absorption efficiency are preferable over the strongly absorbing ones, as they cause less harm to the neighboring healthy tissue. The approximate analytical expressions, derived for the optimal radii in each case, may prove useful in guiding the experimentalists who produce gold nanoshells for plasmonic photothermal therapy of different cancers at their various growth stages.

Acknowledgments

The work of D. Sikdar is supported by the Department of Business and Innovation of the Victorian Government, through its Victoria India Doctoral Scholarship Program (managed by the Australia India Institute). The work of I. D. Rukhlenko and M. Premaratne is supported by the Australian Research Council, through its Discovery Early Career Researcher Award DE120100055 and Discovery Grant scheme under Grant DP110100713, respectively. The work of W. Cheng is supported the Australian Research Council, through its Discovery Grant scheme under Grant DP120100170.

#178972 - $15.00 USD Received 31 Oct 2012; revised 29 Nov 2012; accepted 29 Nov 2012; published 5 Dec 2012